Northumbria Research Link

www.northumbria.ac.uk/nrl

northumbria
UNIVERSITY
University Library

ASTRONOMY
AND
ASTROPHYSICS

A developed stage of Alfvén wave phase mixing

G.J.J. Botha[1]**, T.D. Arber**[2]**, V.M. Nakariakov**[3]**, and F.P. Keenan**[1]

[1] Queen's University, Department of Pure and Applied Physics, Belfast BT7 1NN, UK (gert@math.ucl.ac.uk; f.keenan@qub.ac.uk)
[2] University of St. Andrews, School of Mathematical and Computational Sciences, St. Andrews, Fife KY16 9SS, UK (tda@astro.warwick.ac.uk)
[3] University of Warwick, Department of Physics, Coventry CV4 7AL, UK (valery@astro.warwick.ac.uk)

Abstract. Alfvén wave phase mixing is an extensively studied mechanism for dissipating wave energy in an inhomogeneous medium. It is common in the vast majority of phase mixing papers to assume that even though short scale lengths and steep gradients develop as a result of phase mixing, nonlinear wave coupling does not occur. However, weakly nonlinear studies have shown that phase mixing generates magnetoacoustic modes. Numerical results are presented which show the nonlinear generation of magnetosonic waves by Alfvén wave phase mixing. The efficiency of the effect is determined by the wave amplitude, the frequency of the Alfvén waves and the gradient in the background Alfvén speed. Weakly nonlinear theory has shown that the amplitude of the fast magnetosonic wave grows linearly in time. The simulations presented in this paper extend this result to later times and show saturation of the fast magnetosonic component at amplitudes much lower than that of the Alfvén wave. For the case where Alfvén waves are driven at the boundary, simulating photospheric footpoint motion, a clear modulation of the saturated amplitude is observed. All the results in this paper are for a low amplitude (≤ 0.1), single frequency Alfvén wave and a uniform background magnetic field in a two dimensional domain. For this simplified geometry, and with a monochromatic driver, we concluded that the nonlinear generation of fast modes has little effect on classical phase mixing.

Key words: Magnetohydrodynamics (MHD) – plasmas – waves – Sun: corona

1. Introduction

Magnetohydrodynamic (MHD) waves play an important role in the dynamics of various astrophysical plasma systems. They are key building elements in theories of acceleration of the solar and stellar winds, coronal heating and the formation of inhomogeneities in and support of molecular clouds. Also, in recent times, MHD waves have been observed in the solar wind and the solar corona. Therefore, investigation of the main features of MHD wave dynamics is a significant part of plasma astrophysics. The behaviour of MHD waves in homogeneous plasmas is well understood. However, in astrophysical situations, the wavelength is often of the same order as the characteristic spatial scale of some macro parameters of the plasma (e.g. density, magnetic field, temperature, steady flow). Interaction of MHD waves with plasma inhomogeneities generates a number of very interesting physical phenomena, such as mode coupling, appearance of trapped modes and guided propagation, wave dispersion, resonant absorption and phase mixing (see, e.g. Roberts 1991 and Goossens 1991), which can dramatically affect the MHD wave dynamics and, in particular, cause enhanced dissipation and heating of astrophysical plasmas.

Alfvén wave phase mixing has been studied extensively as a possible mechanism for coronal heating (Heyvaerts & Priest 1983; Browning 1991; Malara et al. 1996; Nakariakov et al. 1997, 1998; De Moortel et al. 1999). Briefly, the idea of the mechanism is simple: when the medium has a density gradient perpendicular to the magnetic field, the Alfvén speed is a function of the transverse coordinate. Consequently, on each magnetic field line, Alfvén waves propagate with their local Alfvén speed. After a certain time, perturbations by Alfvén waves of neighbouring magnetic field lines become out of phase, i.e. there is phase mixing. This effect leads to the generation of smaller and smaller transverse spatial scales. The generation of transverse gradients in the wave leads to a strong increase in the dissipation of Alfvén wave energy due to viscosity and/or resistivity, because the dissipation is proportional to the wave number squared. Throughout this paper we will refer to this model of Alfvén wave phase mixing, which ignores compressible effects and nonlinear wave coupling, as the classical phase mixing model.

For a compressible plasma, an alternative sink of Alfvén wave energy in an inhomogeneous plasma is conversion to the magnetosonic mode, and this mode can propagate across the magnetic field. Alfvén waves are subject to dissipation due to the shear component of the viscosity tensor, while the fast magnetosonic modes are subject to dissipation due to the viscosity tensor's volume component. In the near collisionless plasma of the corona the volume component of the viscosity is much higher than the shear component. As a result fast magnetosonic waves can be dissipated much faster than Alfvén waves and the coupling of Alfvén into fast waves may be an efficient mechanism

for dissipating Alfvén wave energy. This process has been called *indirect heating of the plasma through phase mixing* (Nakariakov et al. 1997). According to weakly nonlinear theory the amplitude of this fast wave component grows linearly in time. Also, because the fast waves propagate across magnetic field lines they can give rise to heating of the plasma away from the initial phase mixing region. This effect leads to thermal transport across the magnetic field, which is very important in the thermodynamics of strongly magnetized plasmas where the usual thermal conduction across the field is depressed. Similar effects were found for phase mixing on inhomogeneous steady flows in plasmas (Nakariakov et al. 1998). In addition, in the almost collisionless plasmas of solar and stellar corona, the obliquely propagating compressive waves can be dissipated by Landau damping (see, e.g. Wentzel 1989).

The analytical results of Nakariakov et al. (1997), showing the secular ($\propto t$) growth of the fast wave perturbations during the initial stage of the phase mixing development, have been obtained under the simplifying assumptions of no dissipation, zero plasma beta and weakly nonlinear coupling. Also, magnetosonic perturbations were assumed to be initially absent from the system. The last assumption restricts the analysis to the early stage of the system's evolution, when the magnetosonic waves are of sufficiently low amplitude. The analytical treatment of the developed stage of phase mixing has not yet been undertaken. However, useful information on MHD wave behaviour can also be obtained by full MHD numerical simulation. There have been several numerical studies undertaken in this direction. Malara et al. (1996) have, through other interesting phenomena, found nonlinear generation of fast magnetosonic waves in the phase mixing region (their runs 7-9). The efficiency of the generation has been estimated as proportional to the square of the Alfvén wave amplitude. However, the relatively low Reynolds numbers (2000) used in the simulations, did not allow the authors to simulate significant phase mixing and, so, to observe the effect of indirect heating. The same effect has also been observed by Ofman & Davila (1997) numerically simulating nonlinear Alfvén waves in coronal holes. On the slopes of the density inhomogeneity associated with the coronal hole, the generation of fast waves has been clearly seen (see, e.g., Fig. 2 of the paper). Also the Lundquist number, the measure of dissipation of short scale perturbations, was low (10^3) in the simulations. Poedts et al. (1997) studied both phase mixing and resonant dissipation in the Solar corona. These simulations showed phase mixing in expanding coronal holes (see Fig. 4 of the paper) but they did not run long enough to reach the strongly phase mixed regime or study nonlinearly generated waves.

In this study, we consider the developed stage of Alfvén wave phase mixing, aiming to determine if the amplitude of the generated fast mode continues to grow linearly or saturates. In addition, effects of weak finite plasma-β are incorporated into the model. We perform 2.5D, time dependent numerical simulations of the ideal MHD set of equations, using the Lagrangian-Eulerian remap technique. The simulations allow us to investigate the effects of the sharp transverse structuring generated by phase mixing.

2. The model and background theory

Our governing equations are from ideal magnetohydrodynamics:

$$\frac{\partial \rho}{\partial t} + \bigtriangledown \cdot (\rho \mathbf{v}) = 0, \tag{1}$$

$$\rho \frac{\partial \mathbf{v}}{\partial t} + \rho(\mathbf{v} \cdot \bigtriangledown)\mathbf{v} + \bigtriangledown p + \mathbf{B} \wedge (\bigtriangledown \wedge \mathbf{B}) = 0, \tag{2}$$

$$\frac{\partial \mathbf{B}}{\partial t} - \bigtriangledown \wedge (\mathbf{v} \wedge \mathbf{B}) = 0, \tag{3}$$

$$\frac{\partial p}{\partial t} + \mathbf{v} \cdot \bigtriangledown p + \gamma p \bigtriangledown \cdot \mathbf{v} = 0, \tag{4}$$

where t is the time, ρ is the plasma density, $\mathbf{v}$ the velocity, p the pressure, $\mathbf{B}$ the magnetic field and $\gamma = 5/3$. All quantities are normalised as $\mathbf{B} = B_* \tilde{\mathbf{B}}$, $p = B_*^2 \tilde{p}/\mu_0$, $\mathbf{r} = a_* \tilde{\mathbf{r}}$, $\rho = \rho_* \tilde{\rho}$, $\mathbf{v} = \sqrt{B_*^2/(\mu_0 \rho_*)}\, \tilde{\mathbf{v}}$ and $t = a_* \sqrt{\mu_0 \rho_*/B_*^2}\, \tilde{t}$, where all the symbols have their usual meanings. To simplify the notation, the tilde has been dropped in Eqs. (1) to (4) as well as in the rest of this paper.

2.1. The equilibrium

We consider these equations in Cartesian coordinates and assume that there are no variations in the y direction ($\partial/\partial y = 0$), thereby reducing the analysis to two dimensions. The equilibrium state is described by a homogeneous magnetic field in the z direction and a density gradient in the x direction:

$$\rho_0 = \rho_0(x) \;;\; p_0 \equiv \text{constant} \tag{5}$$
$$\mathbf{B}_0 = (0, 0, B_0) \;;\; \mathbf{v_0} = \mathbf{0} \tag{6}$$

while the finite amplitude perturbations

$$\rho = \rho(x, z, t) \;;\; \mathbf{v} = (v_x, v_y, v_z) \tag{7}$$
$$p = p(x, z, t) \;;\; \mathbf{B} = (B_x, B_y, B_z) \tag{8}$$

are allowed in the plasma. The equilibrium conditions (5) and (6) allow the unperturbed total pressure to be constant across the magnetic field.

2.2. Analytical description

Following the standard method (Nakariakov et al. 1995, 1997), the MHD equations are written in component form using equilibrium (5) and (6) and perturbations (7) and (8). These equations are correct to an arbitrary order of the perturbations.

$$\frac{\partial \rho}{\partial t} + \rho_0 \left(\frac{\partial v_x}{\partial x} + \frac{\partial v_z}{\partial z} \right) + v_x \frac{\partial \rho_0}{\partial x} = N_1, \tag{9}$$

$$\rho_0 \frac{\partial v_x}{\partial t} + \frac{\partial p}{\partial x} - B_0 \left(\frac{\partial B_x}{\partial z} - \frac{\partial B_z}{\partial x} \right) = N_2, \tag{10}$$

$$\rho_0 \frac{\partial v_y}{\partial t} - B_0 \frac{\partial B_y}{\partial z} = N_3, \tag{11}$$

$$\rho_0 \frac{\partial v_z}{\partial t} + \frac{\partial p}{\partial z} = N_4, \tag{12}$$

$$\frac{\partial B_x}{\partial t} - B_0 \frac{\partial v_x}{\partial z} = N_5, \tag{13}$$

$$\frac{\partial B_y}{\partial t} - B_0 \frac{\partial v_y}{\partial z} = N_6, \qquad (14)$$

$$\frac{\partial B_z}{\partial t} + B_0 \frac{\partial v_x}{\partial x} = N_7, \qquad (15)$$

$$\frac{\partial p}{\partial t} + \gamma p_0 \left(\frac{\partial v_x}{\partial x} + \frac{\partial v_z}{\partial z} \right) = N_8, \qquad (16)$$

with the nonlinear terms given by

$$N_1 = -\rho \left(\frac{\partial v_x}{\partial x} + \frac{\partial v_z}{\partial z} \right) - v_x \frac{\partial \rho}{\partial x} - v_z \frac{\partial \rho}{\partial z}, \qquad (17)$$

$$N_2 = -\rho \frac{\partial v_x}{\partial t} - (\rho_0 + \rho) \left[v_x \frac{\partial}{\partial x} + v_z \frac{\partial}{\partial z} \right] v_x - B_y \frac{\partial B_y}{\partial x}$$
$$+ B_z \left(\frac{\partial B_x}{\partial z} - \frac{\partial B_z}{\partial x} \right), \qquad (18)$$

$$N_3 = -\rho \frac{\partial v_y}{\partial t} - (\rho_0 + \rho) \left[v_x \frac{\partial}{\partial x} + v_z \frac{\partial}{\partial z} \right] v_y + B_z \frac{\partial B_y}{\partial z}$$
$$+ B_x \frac{\partial B_y}{\partial x}, \qquad (19)$$

$$N_4 = -\rho \frac{\partial v_z}{\partial t} - (\rho_0 + \rho) \left[v_x \frac{\partial}{\partial x} + v_z \frac{\partial}{\partial z} \right] v_z$$
$$- B_x \left(\frac{\partial B_x}{\partial z} - \frac{\partial B_z}{\partial x} \right) - B_y \frac{\partial B_y}{\partial z}, \qquad (20)$$

$$N_5 = -\frac{\partial}{\partial z} \left(v_z B_x - v_x B_z \right), \qquad (21)$$

$$N_6 = \frac{\partial}{\partial z} \left(v_y B_z - v_z B_y \right) - \frac{\partial}{\partial x} \left(v_x B_y - v_y B_x \right), \qquad (22)$$

$$N_7 = \frac{\partial}{\partial x} \left(v_z B_x - v_x B_z \right), \qquad (23)$$

$$N_8 = -v_x \frac{\partial p}{\partial x} - v_z \frac{\partial p}{\partial z} - \gamma p \left(\frac{\partial v_x}{\partial x} + \frac{\partial v_z}{\partial z} \right). \qquad (24)$$

Eqs. (9)–(16) describe all the waves occurring in the plasma. By combining these expressions, one obtains for the evolution of the velocity components

$$\left(\frac{\partial^2}{\partial t^2} - c_A^2 \frac{\partial^2}{\partial z^2} \right) v_y = \frac{1}{\rho_0} \left(\frac{\partial N_3}{\partial t} + B_0 \frac{\partial N_6}{\partial z} \right), \qquad (25)$$

$$\left(\frac{\partial^2}{\partial t^2} - c_s^2 \frac{\partial^2}{\partial z^2} \right) v_z - c_s^2 \frac{\partial^2 v_x}{\partial z \partial x} = \frac{1}{\rho_0} \left(\frac{\partial N_4}{\partial t} - \frac{\partial N_8}{\partial z} \right), \qquad (26)$$

$$\left[\frac{\partial^2}{\partial t^2} - (c_s^2 + c_A^2) \frac{\partial^2}{\partial x^2} - c_A^2 \frac{\partial^2}{\partial z^2} \right] v_x - c_s^2 \frac{\partial^2 v_z}{\partial z \partial x} =$$
$$\frac{1}{\rho_0} \left[\frac{\partial N_2}{\partial t} - \frac{\partial N_8}{\partial x} + B_0 \left(\frac{\partial N_5}{\partial z} - \frac{\partial N_7}{\partial x} \right) \right] \qquad (27)$$

where the definitions

$$c_A(x) = \sqrt{\frac{B_0^2}{\rho_0(x)}} \quad ; \quad c_s(x) = \sqrt{\frac{\gamma p_0}{\rho_0(x)}} \qquad (28)$$

have been used. Here $c_A = c_A(x)$ is the Alfvén speed and $c_s = c_s(x)$ the sound speed. Eq. (25) describes the evolution of a linearly polarized Alfvén wave, and the pair of linearly coupled Eqs. (26) and (27) describes the evolution of slow and fast magnetosonic waves. In some limiting cases, e.g. $\beta = 0$, $\partial/\partial x$ or $\partial/\partial z = 0$, the equations for slow and fast modes are decoupled. The wave equations are correct to an arbitrary order of nonlinearity.

In order to obtain expressions for the dependence of the plasma quantities on the perturbed velocities in the model, consider Eqs. (9) to (16) in the linear limit. It follows that

$$\rho = -\int \left[\frac{\partial}{\partial x} (\rho_0 v_x) + \frac{\partial}{\partial z} (\rho_0 v_z) \right] dt, \qquad (29)$$

$$p = -\gamma p_0 \int \left(\frac{\partial v_x}{\partial x} + \frac{\partial v_z}{\partial z} \right) dt, \qquad (30)$$

$$\frac{B_x}{B_0} = \int \frac{\partial v_x}{\partial z} dt, \qquad (31)$$

$$\frac{B_y}{B_0} = \int \frac{\partial v_y}{\partial z} dt, \qquad (32)$$

$$\frac{B_z}{B_0} = -\int \frac{\partial v_x}{\partial x} dt. \qquad (33)$$

In the geometry considered, a linear Alfvén wave perturbs v_y and B_y, while the magnetosonic waves perturb the remaining physical quantities. However, in the nonlinear regime, the linearly polarized Alfvén wave perturbs these quantities too, and this leads to nonlinear excitation of the magnetosonic waves and to consequent coupling of the Alfvén wave to the magnetosonic perturbations. In other words, this process is self-interaction of the Alfvén wave.

The initial stage of nonlinear generation of magnetosonic waves by Alfvén waves in an inhomogeneous medium has been considered by Nakariakov et al. (1997). To estimate the efficiency of this process, we consider a zero-β plasma of the geometry described above. This case is described by Eqs. (25)–(27) with $c_s = 0$. Initially, there is an Alfvén wave only, perturbing B_y and v_y, and all remaining physical quantities are not perturbed. So, initially, all the nonlinear terms on the right hand side of Eq. (25) are zero, and the Alfvén wave evolves linearly, according to the left hand side of (25). (Note that the same equation has been derived by Ofman & Davila 1997). As B_y is nonzero, the terms N_2 and N_4 are non-zero too, which give source terms on the right hand sides of (26) and (27). Consequently, the magnetosonic perturbations are generated as

$$\frac{v_z}{c_A} \sim \frac{1}{2} \left(\frac{B_y}{B_0} \right)^2, \qquad (34)$$

$$\frac{v_x}{c_A} \sim \frac{1}{4} \frac{dc_A}{dx} \left(\frac{B_y}{B_0} \right)^2 t. \qquad (35)$$

Both motions in the x and z directions perturb the density. The longitudinal motions (v_z) are always generated by an Alfvén wave, while the transverse perturbations (v_x) are connected with the inhomogeneity of the medium in the transverse direction, dc_A/dx. In the initial stage, the transverse perturbations are

generated secularly ($\propto t$) because of phase mixing of Alfvén waves. In the cold case, the transverse perturbations correspond to obliquely propagating fast magnetosonic waves, and the longitudinal perturbations to degenerated slow waves.

In the case of warm plasma ($c_s \neq 0$), slow and fast magnetosonic waves are coupled with each other by the pair of Eqs. (27) and (26). In other words, each wave, slow or fast, perturbs both v_x and v_z components of the velocity. However, the longitudinal and transversal components of the velocity are excited by the same mechanisms (34) and (35) as in the cold case.

The developed stage of the nonlinear interaction of Alfvén waves with compressive perturbations is characterized by the back-reaction of the induced compressive perturbations on the Alfvén waves. Technically, this phenomenon is connected with the growth of the nonlinear terms on the right hand side of Eq. (25). In the case of a homogeneous medium, the self-interaction of Alfvén waves is described by the Cohen–Kulsrud equation (Cohen & Kulsrud 1974, see also discussions in Ofman & Davila 1995, Verwichte et al. 1999 and Nakariakov et al. 2000). However, this effect is proportional to the square of the Alfvén wave amplitude and can significantly influence the wave evolution only if the wave amplitude is sufficiently high or the wave propagates over sufficient long distances to allow the nonlinear effects to build up.

Thus, in numerical simulations, we expect to observe weakly nonlinear coupling of Alfvén modes with fast and slow magnetosonic modes during the initial stage of the wave interaction described by Eqs. (34) and (35).

3. The numerical code

The code used to produce the results (*Lare2d*) was developed at St. Andrews University by Arber et al. (2000). *Lare2d* is a numerical code that operates by taking a Lagrangian predictor-corrector time step and after each Lagrangian step all variables are conservatively remapped back onto the original Eulerian grid using Van Leer gradient limiters. Results are obtained by initializing the code with the unperturbed density

$$\rho_0(x) = 3 - 2\tanh(\alpha x), \tag{36}$$

where α is a free parameter used to fix the scale length of the density inhomogeneity. An example with $\alpha = \sqrt{0.05}$ is shown in Fig. 1. This is the value of α used throughout unless otherwise explicitly stated. Note, that the position of the highest gradient in the Alfvén speed ($c_A = B_0/\sqrt{\rho_0(x)}$) is shifted toward the positive x with respect to the positioning of the highest gradient in the density ($x = 0$).

The boundary condition in the x direction is that all quantities have zero gradient. The x boundaries are far away from the maximum background density change at $x = 0$, so that they do not influence the physics.

In this geometry linearly polarized Alfvén waves perturb the y components of the magnetic field and velocity (B_y and v_y). This is implemented numerically in two different ways:
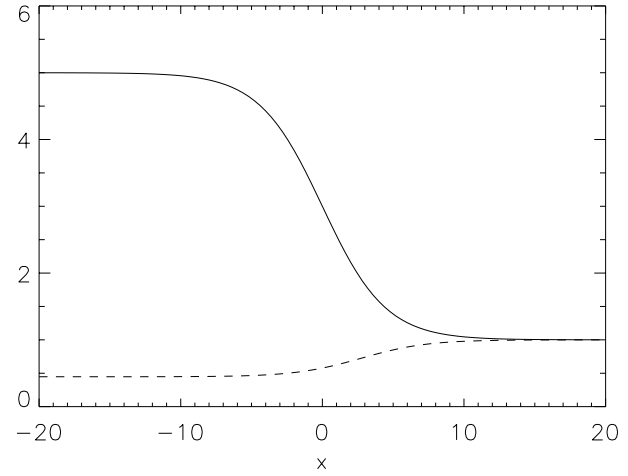

Fig. 1. Profiles of the unperturbed density $\rho_0(x)$ (*solid curve*) and Alfvén speed (*dashed curve*) for the inhomogeneity parameter $\alpha = \sqrt{0.05}$.

Firstly, the z direction is treated as periodic and an Alfvén wave with amplitude 0.001 is initialized so that two wavelengths fit into the numerical domain. The wave is planar at $t = 0$ with wave-fronts parallel to the x axis. (Sect. 4)

Secondly, a sinusoidal Alfvén wave is driven at the $z = 0$ boundary: $v_y(x, z, t) = A \sin \omega t$. Again the amplitude is $A = 10^{-3}$ and driving frequency is $\omega = 1$. The driven Alfvén wave propagates in the z direction and as soon as the wave reaches the upper boundary the simulation is stopped. (Sect. 5)

A plasma-β of 0.01 is used, to correspond to the plasma in the solar corona. Unless otherwise stated, the initialization described in this section has been used for all the numerical simulations presented in this paper.

Previous phase mixing calculations (De Moortel et al. 1999) have used scale lengths and speeds estimated for coronal plumes. One of the aims of this work is to estimate the relative importance of nonlinear generation of fast modes, as opposed to classical phase mixing, as a mechanism for dissipating Alfvén wave energy. A typical plume in this paper is assumed to have a number density of $4 \times 10^{15} m^{-3}$, $B = 10G$, $T = 10^6 K$ and a background density of $10^{15} m^{-3}$. An increase in density by a factor of 4 is assumed to take place over a distance of $7 Mm$. ($1 Mm = 10^6 m$.) For these parameters a one minute period Alfvén wave would have a wavelength $\simeq 30 Mm$, while five minute oscillations would have wavelengths $\simeq 150 Mm$. Furthermore for the one minute oscillations it is expected (De Moortel et al. 1999) that phase mixing will become prevalent at around 1.5 solar radii. For coronal plumes this suggests that the Alfvén wave is of the order of 10 full wavelengths out of phase when classical phase mixing is significant. Simulations in this work are therefore for density scale lengths less than the Alfvén wavelength, with a density increase by a factor of four, and run for sufficient time that the waves go out of phase by 10 wavelengths across the density ramp.
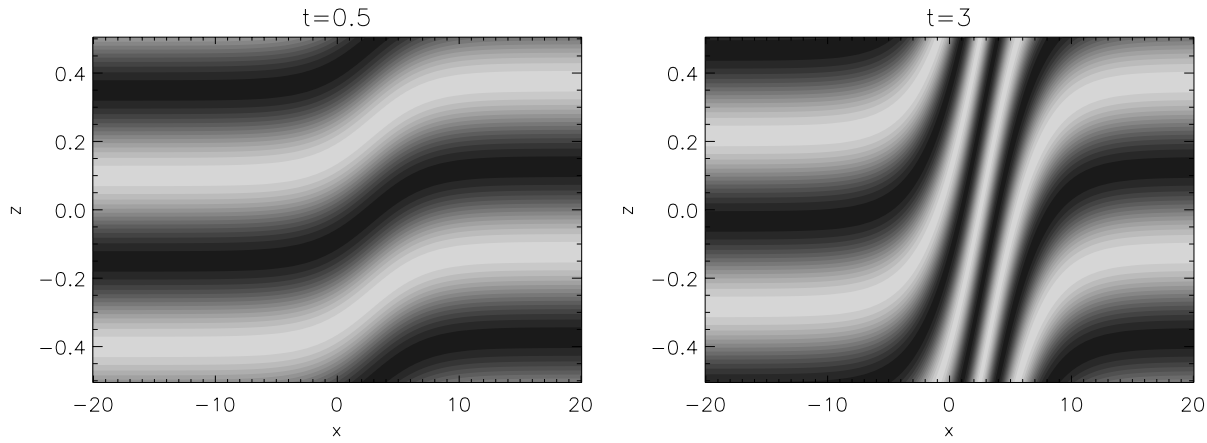
Fig. 2. A contour plot of the Alfvén wave. The B_y amplitude is plotted on the (x, z) plane at times t=0.5 and t=3.

4. Saturation levels of magnetosonic waves

The numerical results obtained using a periodic z direction – the direction of the uniform magnetic field B_0 – are presented in this section. An Alfvén wave is initialized at $t = 0$ and the simulation then evolves from that state without further Alfvén wave driving, i.e. at $t = 0$ we set $B_y = a \sin(kz)$ and $v_z = a \sin(kz)/\rho^{1/2}$.

As the numerical code evolves in time, the Alfvén wave moves at different local speeds due to the ρ_0 gradient (Fig. 1). Throughout the numerical simulation the Alfvén wavelength λ_A stays practically constant (the nonlinear modification of the Alfvén wavelength is insignificant in this study because the amplitude is weak and the Alfvén waves remain practically linear, see the discussion in Sect. 2.2), so that phase mixing of the Alfvén waves takes place where the background density gradient (and hence the local Alfvén velocity) changes. Fig. 2 presents two contour plots of the (x, z) plane in the beginning of the run and at time t=3. These show the phase mixing region centred to the right of $x = 0$ as expected from Fig. 1.

Slow magnetosonic waves are generated nonlinearly by the Alfvén wave. These are generated at every position in the x direction. Fast magnetosonic waves are generated where the phase mixing of the Alfvén wave occurs. The amplitude of the fast magnetosonic waves grows linearly with time during the initial stages of the numerical runs. However, they soon saturate at levels that are dependent on the amplitude and wavelength of the Alfvén wave, as well as the scale length of the background density gradient. The saturation levels of the slow and the fast magnetosonic waves are independent of the plasma-β.

Fig. 3 shows that as the background density scale length decreases, i.e. α increases, the initial rate of linear growth of v_x increases. Note that Figs. 3 and 4 are plots of the maximum value of v_x along the line $x = 0$ versus time and not plots of v_x at a point. In all cases the amplitude still saturates at a low level compared to the Alfvén wave component (which has an amplitude of 10^{-3}). Lower values of α show linear growth of the v_x amplitude for longer and end with a larger saturated amplitude. However, decreasing α by two orders of magnitude only approximately doubles the maximum v_x amplitude. Fig. 4 shows that the initial linear growth of the v_x amplitude is influenced by
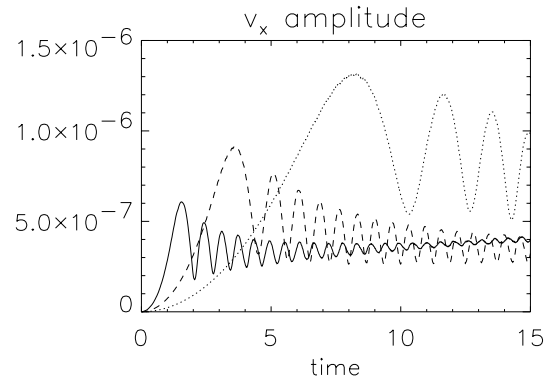

Fig. 3. Time evolution of the fast magnetosonic wave (v_x) amplitude as a function of the background density gradient parameter α. Lines are for $\alpha = \sqrt{0.05}$ (*dotted curve*), $\alpha = \sqrt{0.5}$ (*dashed curve*) and $\alpha = \sqrt{5}$ (*solid curve*).
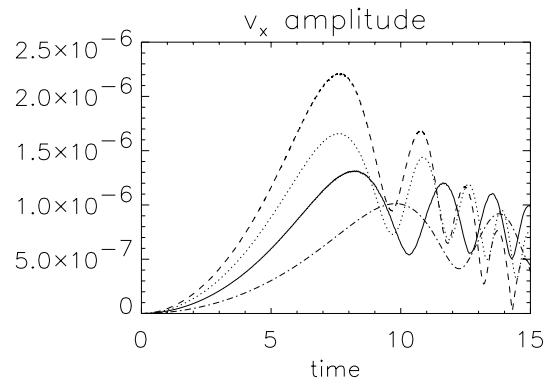
Fig. 4. Time evolution of the fast magnetosonic wave (v_x) amplitude as a function of the Alfvén wave length λ_A. Lines are for $\lambda_A = 0.25$ (*dashed curve*), $\lambda_A = 0.3$ (*dotted curve*), $\lambda_A = 0.5$ (*solid curve*) and $\lambda_A = 1$ (*dot-dashed curve*).

the Alfvén wavelength: shorter Alfvén waves causes stronger growth. Once the v_x amplitude has saturated, there is little distinction between the different Alfvén wavelengths. Fig. 5 shows that the saturated amplitude varies as the square of the Alfvén amplitude.
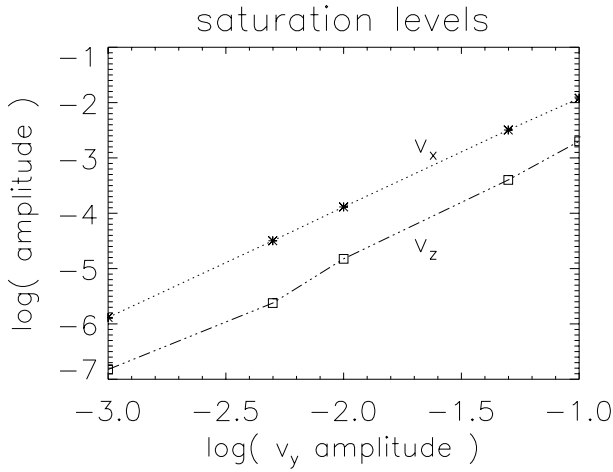
Fig. 5. The saturation levels of the fast (v_x) and slow (v_z) magnetosonic wave amplitudes as a function of the Alfvén wave (v_y) amplitude.

It is the gradient in the x direction of v_y which is the source of the fast waves. Initially this is zero but grows linearly in time due to phase mixing. This linear growth of the gradient continues throughout the simulations presented in this paper, i.e. there is no saturation of the basic phase mixing process. The natural questions which then arise are why does the amplitude of the fast wave not also continue to grow linearly and why does it saturate at the level it does? A possible explanation of this can be given in terms a greatly simplified model. From the full simulations it is clear that the fast wave saturates at low amplitude (typically proportional to the square of the Alfvén wave amplitude). To a good approximation we can then assume that the phase mixing acts as a source of fast waves without perturbing the Alfvén waves. We therefore represent the generation of fast waves by the generation of 1D sound waves (or fast waves if P is interpreted as a magnetic pressure) with a specified driving term, $h(x)$. In this case $h(x)$ is the pressure gradient resulting from phase mixing, i.e. it represents the $B_y \partial B_y / \partial x$ term in Eq. (18) at a fixed point in z. The simplified equations are then

$$\frac{\partial v}{\partial t} + \frac{\partial P}{\partial x} = h(x), \tag{37}$$

$$\frac{\partial P}{\partial t} + \frac{\partial v}{\partial x} = 0, \tag{38}$$

where $h(x)$ is determined from the gradient of B_y^2 with $B_y = a \cos(\omega t)$ and $\omega = \omega_0 / \sqrt{3 - 2\tanh(\alpha x)}$. The advantages of this simplified model are that it contains a driver consistent with the full equations but the only other process included is simple linear wave propagation. Results from this model can therefore only be attributed to the interference of linear waves and it removes any possibility of nonlinear wave interactions being an explanation of the derived solution. This is unlike the full set of MHD equations where all possible ideal MHD process are included. Eqs. (37) and (38) are solved numerically using a second order Maccormack scheme. Fig. 6 shows $h(x)$ and v at three times in the solution. The top figures show that the driving term $h(x)$ has the required properties of a transverse gradient

generated by phase mixing: the amplitude is growing linearly in time and the number of oscillations in the x direction also increases secularly. The bottom figures show that the amplitude of the generated waves has grown linearly in time but then saturates. This can be seen more clearly in Fig. 7 which shows the solution for v as a function of time at $x = 0$. All of these results were produced with $\omega_0 = 5$, $\alpha = 1$ and $a = 0.1$. Varying a confirmed that the saturated amplitude scales as a^2 which is also in agreement with the full MHD results. Calculating the maximum v, $|v|^{max}$ when α is varied does not produce results in clear agreement with the results of Fig. 3. With $a = 0.001$ and $\alpha = 0.05$ this simple model gives $|v|^{max} = 1.6 \times 10^{-6}$, while $\alpha = 0.5$ gives $|v|^{max} = 2.01 \times 10^{-6}$ and $\alpha = 5$ gives $|v|^{max} = 4.78 \times 10^{-7}$. Thus the general behaviour between $\alpha = 0.05$ and $\alpha = 5$ is consistent with the full simulations, i.e. as the density scale length increases the final saturated amplitude increases, but the scaling over this range is not the same as found from the full MHD equations.

From these model equations a natural interpretation of the saturation of fast wave generation by Alfvén waves follows from simple wave interference. At early times there is a single maximum in $h(x)$ whose amplitude grows linearly in time. This generates right and left propagating waves whose amplitudes also grow linearly in time. However, at later times there are many peaks in $h(x)$ and while each of these is growing in amplitude neighbouring peaks are not in phase, i.e. their separation is not an integer multiply of the generated wave's wavelength. Indeed, since the number of maxima in $h(x)$ grows and their separation decreases, it is impossible for these to be coherent emitters of fast waves. Thus while the phase mixing continues to generate shorter and shorter scale lengths the generated fast wave amplitude saturation occurs soon after the phase difference across the density ramp generates a second maximum in the transverse gradient of v_y^2.

5. Results with Alfvén wave driven at $z = 0$

In this section a sinusoidal Alfvén wave is driven at the $z = 0$ boundary. In order to prevent the x boundaries influencing the solution where the phase mixing occurs, the x axis is lengthened to $x \in [-50, 50]$ and the ρ_0 profile of Fig. 1 is shifted so that $\rho_0 = 3$ is at position $x = 25$.

Fig. 8 shows the oblique propagating fast wave generation by phase mixing. The Alfvén wave generated at $z = 0$ propagates in the direction of increasing z values and experiences phase mixing. Fig. 8 presents the generation of transversal gradients in the initially plane Alfvén wave. The gradients are confined to the region where the Alfvén speed experience the variation. These gradients are a source term on the right hand side of Eq. (27). The fast waves excited by the source, propagate across the field with the fast magnetosonic speed $\sqrt{c_s^2 + c_A^2}$, also shown by Fig. 8. Initially the fast wave growth rate is high, according to previous theoretical expectations. However, it saturates later during the simulation and the fast wave amplitude exhibits periodic modulations. Only every fourth point in each direction was used to produce Fig. 8 as this gave the clearest
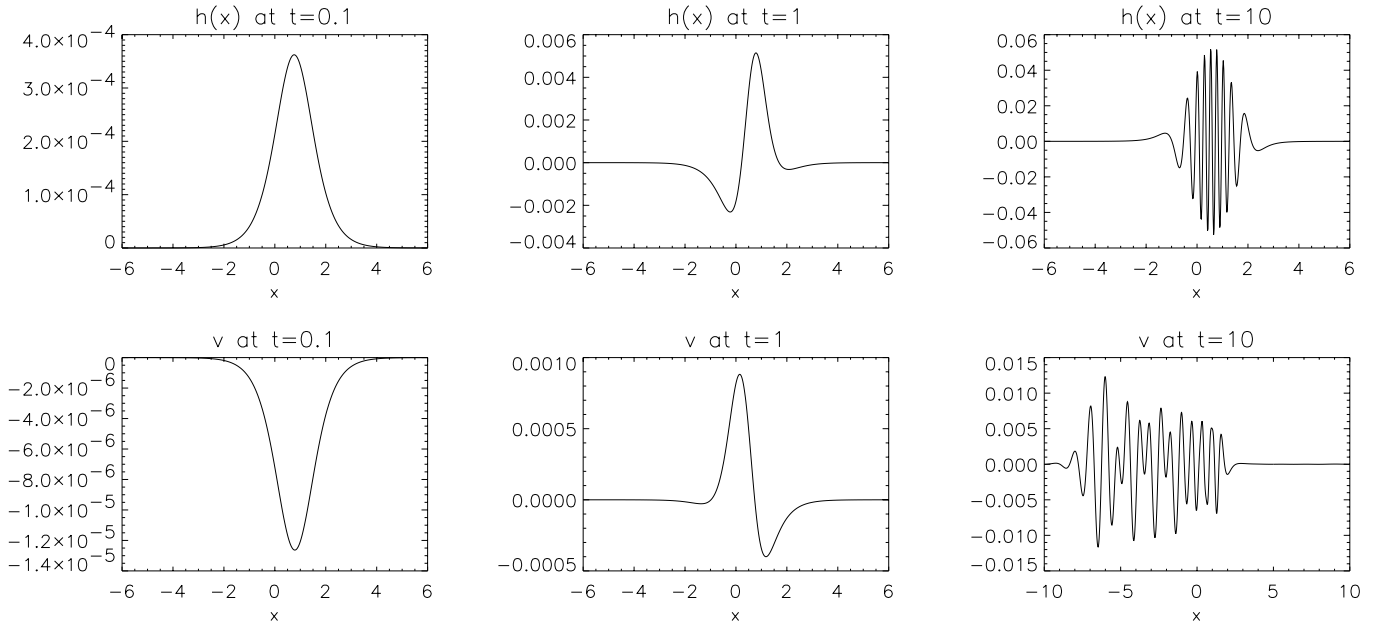
Fig. 6. Plots of $h(x)$ and v from the solution to Eqs. 37 and 38 at $t = 0.1$, $t = 1$ and $t = 10$.

images. All structures are resolved in these simulations even though some of this resolution is clearly lost in using only one out of 16 available data points.

Fig. 9 contains the oscillations of the driven Alfvén wave (B_y and v_y) along the z axis at $x = 25$, as well as the magnetosonic waves generated by the driven wave (B_x, B_z, v_x and v_z). The time during the simulation can be read directly from the z axis using the relation $t = z/c_A$ where c_A is a constant in the z direction, so that as z increases, the time increases. Note that because the amplitudes of the fast and slow magnetosonic components saturate at such a low amplitude there is only a small leakage of energy from the Alfvén wave component into these modes. Thus v_y and B_y in Fig. 9 appear as constant amplitude oscillations because the decrease in amplitude of these components is too small to be apparent from these plots.

By performing a linear analysis similar to Nakariakov et al. (1995, 1997) on the MHD Eqs. (1) to (4) using the ground state (5) and (6), it is easy to show that the oscillations in B_x, B_z, v_x and v_z are double the driven frequency ω. Eqs. (31) and (33) show that the oscillations of B_x and B_z are determined by the behavior of v_x in the linear limit.

Fig. 9 shows the Alfvén wave (B_y and v_y) propagating in the direction of the magnetic field. At the start of the numerical run the driven amplitude is ramped up to 0.001 over 4 wavelengths. The oscillations in v_z show the progress of a sound wave. Up till $z = 30$ the oscillations are centered around zero, and in front of the sound wave the oscillations are positive. The interpretation of this phenomenon is trivial: there are two kinds of the longitudinal motions in the system. The first is produced by a slow wave. They are generated by the driver at $z = 0$ and propagate to $z > 0$ with the sound speed $c_s = \sqrt{\gamma p_0/\rho_0(x)} = \sqrt{0.05/3}$, which gives $z = 30$ at $t = 410$. These perturbations are regular acoustic waves with positive and negative motions of the plasma
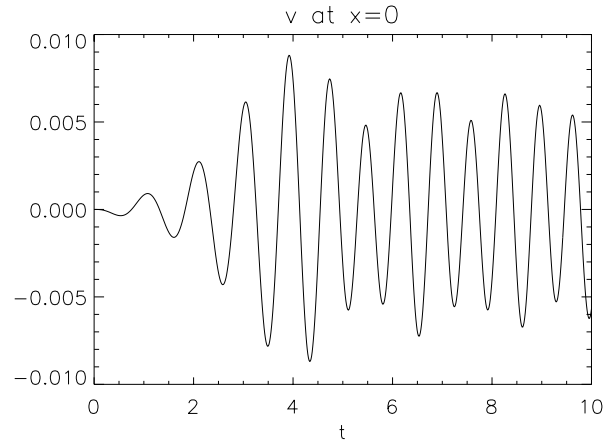

**Fig. 7.** v as a function of time at $x = 0$.

along the field. The second type of the longitudinal perturbations is driven by the Alfvén wave ponderomotive force (see (34)) and are always positive for an Alfvén wave propagating in the positive direction of z. These nonlinearly driven motions propagate with the Alfvén wave speed $c_A = B_0/\sqrt{\rho_0(x)} = 1/\sqrt{3}$ and exist even when $\beta = 0$ (see Verwichte et al. 1999; Nakariakov et al. 2000 for more detailed discussion). At time $t = 410$ the Alfvén wave has traveled to position $z = 236$ along the z axis.

The $z = 0$ boundary conditions on the velocity components are $v_x = 0$, $v_z = 0$ and $v_y = A \sin(\omega t)$. Zero gradient conditions are used on the magnetic field components. These conditions do not drive a pure Alfvén wave but also generate an acoustic wave component. This driven acoustic wave has an amplitude which is proportional to the square of the Alfvén wave. It should be pointed out that the generation of this acoustic wave is by no means an error in the boundary conditions or in the simu-
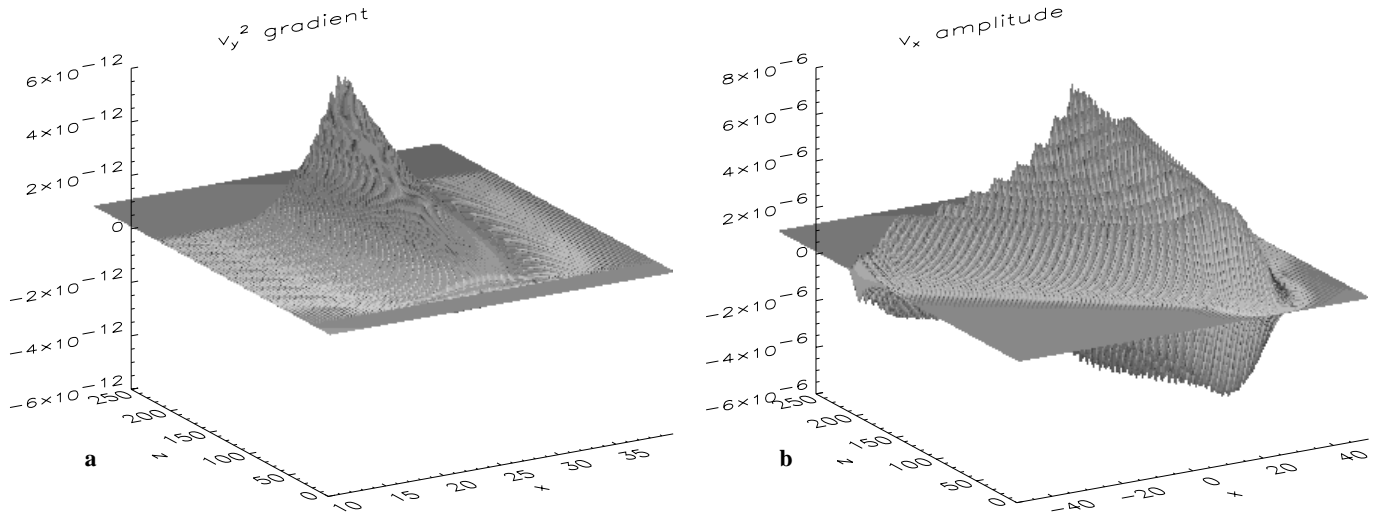
Fig. 8. The growth of (**a**) transverse gradients $\partial v_y^2/\partial x$ in the Alfvén wave due to phase mixing and (**b**) induced fast mode perturbations v_x. Here the Alfvén wave is driven at $z = 0$.
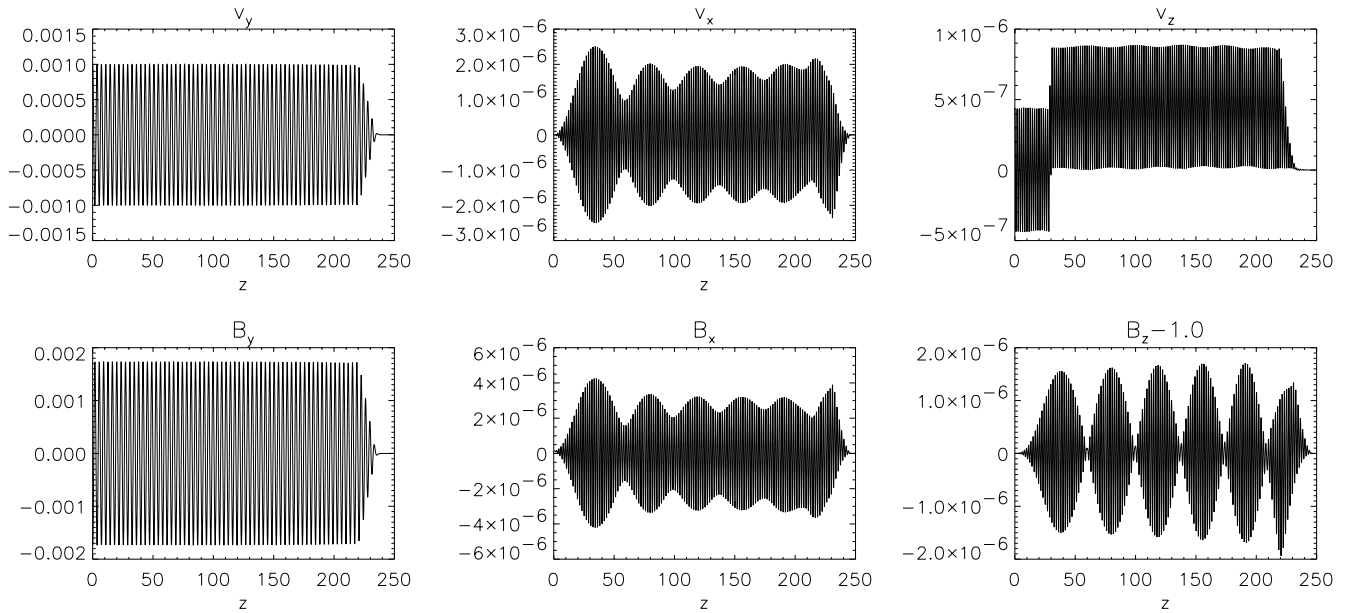

Fig. 9. z profiles at time $t = 410$ of the Alfvén wave (B_y and v_y), fast magnetosonic wave (B_z, B_x and v_x), and the slow magnetosonic wave (v_z).

lation's validity. Photospheric motions will not be generators of pure Alfvén waves and all that is required of driving conditions is that they are physically realistic. The presence of boundary driven acoustic modes does of course introduce another wave into the full set of coupled MHD equations. However, this mode is a second order effect and will not significantly affect the primary Alfvén wave phase mixing. Furthermore, by looking at the results of Fig. 9 beyond $z = 30$, or the periodic boundary results of Sect. 4, we can see the result of phase mixing without this acoustic mode.

The amplitude of v_x saturates (as shown is Sect. 4) and after saturation it experiences a smooth modulation, the wavelength of which is independent of the driven amplitude. The other pa-

rameters that can be changed in the numerical simulation are the frequency ω of the driven Alfvén wave and the unperturbed density ρ_0 gradient. Fig. 10 shows the dependency of the modulation wavelength λ on both these parameters. As the driven wavelength is doubled (i.e. ω is halved) λ doubles in length. When the characteristic length scale is doubled, i.e. α is halved, the wavelength of the modulation λ increases by 3/2.

This modulation, which is also present in the periodic results shown in Fig. 3, is both unexpected and as yet unexplained. A natural interpretation would be that the nonlinearly generated fast mode is beating with some other boundary driven or generated wave. However, in this 2D geometry with a non-sheared magnetic field, this equilibrium cannot support ideal
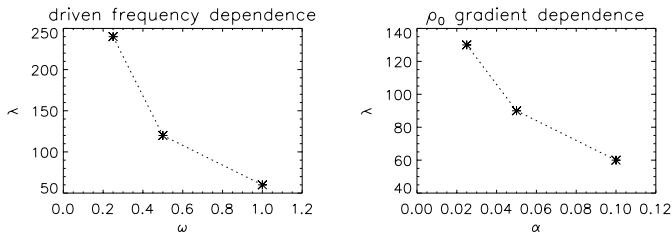
Fig. 10. Dependence of the modulation in the v_x wavelength λ on the driven frequency ω and on α.

MHD trapped fast waves if $\beta < 1$ (Roberts 1981) and we see no evidence of the localized structure (in the x direction) that might be expected from a driven quasi-mode (Poedts & Kerner 1991). This leaves no clear candidate to explain this modulation and we must defer its explanation to a later study.

6. Conclusion

In a transversally inhomogeneous plasma, Alfvén waves are subject to phase mixing (Heyvaerts & Priest 1983). This phenomenon leads to the linear growth of transversal gradients in Alfvén waves, producing a varying magnetic pressure which is the source of fast magnetosonic waves. Phase mixing of a harmonic Alfvén wave excites fast magnetosonic waves at double the frequency of the Alfvén wave (Nakariakov et al. 1997). This analytical result was confirmed by the numerical simulation of a plane Alfvén wave in a two-dimensional domain. It was shown that the fast magnetosonic wave amplitude saturates and experiences a slow modulation, which is a function of the background Alfvén speed gradient and the frequency of the driven wave.

The fast magnetosonic waves, generated continuously by Alfvén wave phase mixing, propagate across the magnetic field, away from the layer of phase mixing. There is therefore a permanent leakage of energy away from the phase mixing layer. This can cause *indirect heating of the plasma through phase mixing* when the obliquely propagating fast waves, excited by Alfvén wave phase mixing, are dissipated at some distance from the layer of phase mixing. This mechanism leads to the spreading out of the heated plasma region from the inhomogeneous layer. However, the results in this paper have shown that the nonlinearly generated fast wave component saturates at an amplitude proportional to the square of the Alfvén wave amplitude. Thus for Alfvén waves generated continuously by photospheric motions, which would have a typical amplitude of 10^{-3} in the normalization of this paper, only a small fraction of the Alfvén wave energy is radiated away as fast waves. We thus conclude that the classical model of phase mixing is valid despite its ignoring nonlinear wave coupling. The picture is different for Alfvén waves with a large amplitude, as might be excited by the shocks emanating from flares. With Alfvén amplitudes of 0.1 the fast mode amplitude would saturate at approximately 0.01. Since the phase mixing mechanism requires the Alfvén waves to propagate out until they are about 10 full wavelengths out of phase before significant phase mixing damping occurs, the transfer of energy into fast waves would be a significant sink

of energy in this case. Also, the saturation level of the compressive perturbations generated by the transversal gradients in the Alfvén wave (v_x) is 2 to 3 times higher than the longitudinal compressive components of the Alfvén wave (v_z). This can strongly affect self-interaction of the Alfvén wave through its generation of compressive perturbations, as discussed in Sect. 2.

The model we have used for phase mixing in this paper is greatly simplified compared to the reality of coronal plumes. We have assumed 2D geometry, a uniform magnetic field, simple density structure and a monochromatic source of Alfvén waves. These are all clear limitations of the model. However, this set of simplifying assumptions is entirely consistent with the great majority of work on phase mixing and thus we were able to directly comment on the applicability of simpler models which ignore nonlinear wave coupling. We have also presented a simplified model as a possible explanation of the results. The saturation of fast waves was then interpreted as destructive interference from incoherent sources. This mechanism is effective to a large extent due to the restrictive geometry of these simulations. If the y coordinate in this work were not ignorable the possibility would exist for constructive interference in other directions. Thus while this work can be definitive in its support for classical phase mixing theories in this simplified geometry a conclusive answer for general frequency drivers and realistic geometries must wait until more detailed study of geometric effects, nonharmonic drivers etc. has been completed.

References

Arber T.D., Longbottom A.W., Gerrard C.L., Milne A.M., 2000, submitted to J. Comput. Physics.
Browning P.K., 1991, Plasma Physics and Controlled Nuclear Fusion 33, 539
De Moortel I., Hood A.W., Ireland J., Arber T.D., 1999, A&A 346, 641
Cohen R.H., Kulsrud R.M., 1974, Phys. Fluids 17, 2215
Goossens M., 1991, In: Priest E.R., Hood A.W. (eds.) Advances in Solar System Magnetohydrodynamics. Cambridge Univ. Press
Heyvaerts J., Priest E.R., 1983, A&A 117, 220
Malara F., Primavera L., Veltri P., 1996, ApJ 459, 347
Nakariakov V.M., Ofman L., Arber T.D., 2000, A&A 353, 741
Nakariakov V.M., Oraevsky V.N., 1995, Solar Physics 160, 289
Nakariakov V.M., Roberts B., Murawski K., 1997, Solar Physics 175, 93
Nakariakov V.M., Roberts B., Murawski K., 1998, A&A 332, 795
Ofman L., Davila J.M., 1995, Journal of Geophysical Research 100, 23; 427
Ofman L., Davila J.M., 1997, ApJ 476, 357
Poedts S., Kerner W., 1991, Phys. Rev. Lett. 66, 2871
Poedts S., Tóth G., Beliën A.J.C., Goedbloed J.P., 1997, Solar Physics 172, 45
Roberts B., 1981, Solar Physics 69, 27
Roberts B., 1991, In: Priest E.R., Hood A.W. (eds.) Advances in Solar System Magnetohydrodynamics. Cambridge Univ. Press
Verwichte E., Nakariakov V.M., Longbottom A., 1999, J. Plasma Phys. 62, 219
Wentzel D.G., 1989, ApJ 336, 1073